AIAA JOURNAL
Vol. 30, No. 3, March 1992

Finite Element Analysis of Composite Structures Containing Distributed Piezoceramic Sensors and Actuators

Sung Kyu Ha,* Charles Keilers,† and Fu-Kuo Chang‡
Stanford University, Stanford, California 94305

A finite element formulation is presented for modeling the dynamic as well as static response of laminated composites containing distributed piezoelectric ceramics subjected to both mechanical and electrical loadings. The formulation was derived from the variational principle with consideration for both the total potential energy of the structures and the electrical potential energy of the piezoceramics. An eight-node three-dimensional composite brick element was implemented for the analysis, and three-dimensional incompatible modes were introduced to take into account the global bending behavior resulting from the local deformations of the piezoceramics. Experiments were also conducted to verify the analysis and the computer simulations. Overall, the comparisons between the predictions and the data agreed fairly well. Numerical examples were also generated by coupling the analysis with simple control algorithms to control actively the response of the integrated structures in a closed loop.

Introduction

BECAUSE of their coupled mechanical and electrical properties,[1-3] piezoelectric ceramics have recently attracted significant attention for their potential application as sensors for monitoring and as actuators for controlling the response of structures. The concept of using a network of actuators and sensors to form a self-controlling and self-monitoring "smart" system in advanced structural design has drawn considerable interest among the research community. This new technology could possibly be applied to the design of large-scale space structures, aircraft structures, satellites, and so forth.[4,5]

Additionally, recent advances in design and manufacturing technologies have greatly enhanced the use of advanced fiber-reinforced composite materials for aircraft and aerospace structural applications. As a consequence, the integration of composite structural design with the "smart system" concept could potentially result in significant improvement in the performance of aircraft and space structures. Numerous investigators have recently demonstrated the feasibility of the integrated concept through the use of simple structures such as cantilever beams.[6-10] Several analyses and numerical models have also been developed to analyze the integrated structures.[6-14] Most of the numerical models were based on the Ritz approach and focused on simplified structures under simple loading conditions. Although finite element methods have been developed for piezoelectrics structures,[15-16] the use of finite element techniques for analyzing the integrated piezo-composite structures has not been fully established. To advance this technology further for more complicated and large-scaled structures, a thorough and comprehensive development in theory and numerical methods is critically important and essentially needed.

Therefore, the objective of this investigation was to develop a finite element analysis for modeling the mechanical-electrical response of fiber-reinforced laminated composite structures containing distributed piezoceramics under static as well as dynamic mechanical or electrical loadings. A finite element code, designated as "COMPZ," was developed on the basis of the analysis during this investigation. Experiments using T300/976 composites and PZT G1195N piezoelectric ceramics were also conducted to verify the analysis and the computer simulations. Numerical examples were performed by implementing simple control algorithms into the code in such a way that the sensor outputs predicted by the code could be used to determine the amount of input to the actuators for controlling the response of the integrated structures in a closed loop.

Received April 12, 1991; revision received July 15, 1991; accepted for publication July 22, 1991. Copyright © 1991 by the American Institute of Aeronautics and Astronautics, Inc. All rights reserved.

*Postdoctoral Researcher, Department of Aeronautics and Astronautics.
†Graduate Student, Department of Aeronautics and Astronautics.
‡Associate Professor, Department of Aeronautics and Astronautics. Member AIAA.

Statement of the Problem

Consider a fiber-reinforced laminated composite plate containing distributed piezoelectric ceramics as sensors or actuators that can be bonded on the surfaces or embedded inside the structure as shown in Fig. 1. The ply orientation and thickness of the laminate can be arbitrary. It was desired to determine the mechanical response of the structure as well as the local sensor electrical outputs for given proper mechanical loading condition on the structure or electrical potential on the actuators.

Model

The mechanical and electrical response of piezoelectric ceramics can be described by the equation of motion

$$\sigma_{ji,j} + f_i = \rho \ddot{u}_i \tag{1}$$

and the Maxwell's equation (assuming electrically polarized, unmagnetized, and charge free media)

$$D_{i,i} = 0 \tag{2}$$

where σ_{ij}, f_i, ρ, $\ddot{u}_i$, u_i, and D_i are stresses, body force in a unit volume, density, accelerations, displacements, and electric displacements,[1-3] respectively.

The constitutive equations of the piezoceramics can be expressed as[1-3]

$$\varepsilon_{ij} = S^E_{ijkl}\sigma_{kl} + d_{kij}E_k \tag{3}$$

and

$$D_i = d_{ikl}\sigma_{kl} + \xi^\sigma_{ij}E_j \tag{4}$$

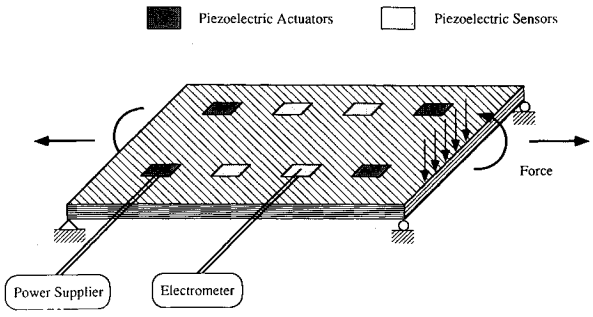

Fig. 1 Composite plate with distributed piezoceramic sensors and actuators.

where S^E_{ijkl} are elastic compliances for a constant electric field, ξ^σ_{ij} are the permittivities for a constant elastic stress, and d_{ijk} are the piezoelectric strain constants. E_i are the electric field components.

The strain-displacement relations for small deformations can be written as

$$\varepsilon_{ij} = 1/2(u_{i,j} + u_{j,i}) \tag{5}$$

and the electric field E_i is related to the electric potential V by

$$E_i = -V_{,i} \tag{6}$$

The complete solutions of Eqs. (1–6) can describe the mechanical and electrical state of the piezoelectrical ceramics, provided that proper boundary and initial conditions are given. For laminated composites, the equation of motion, Eq. (1), is also valid, and the constitutive equation of a unidirectional composite can be described by the following form:

$$\varepsilon_{ij} = S_{ijkl}\sigma_{kl} \tag{7}$$

where S_{ijkl} are the elastic compliances of the composites.[17, 18]

Based on the variational principle, Eqs. (1) and (2) multiplied by the corresponding variations and integrated over the entire domain of the integrated structure result in

$$\int_v (\sigma_{ij,j} - \rho\ddot{u}_i)\delta u_i \, dv + \int_{v_p} D_{i,i}\delta V \, dv = 0 \tag{8}$$

where v and v_p stand for the entire volume including composites and piezoceramics, and the volume of piezoelectric ceramics, respectively. Here, the body forces f_i are neglected.

According to the divergence theorem, Eq. (8) can be rewritten as

$$\int_v \rho\ddot{u}_i\delta u_i\delta v + \int_v \sigma_{ij}\delta\varepsilon_{ij} \, dv - \int_{v_p} D_i\delta E_i \, dv = \int_A T_i\delta u_i \, dA + \int_{A_p} Q\delta V \, dA \tag{9}$$

where T_i are surface tractions applied on the surface A, and Q is the electrical charge applied on the surface A_p of the piezoceramic actuators.

By introducing the new extended displacements and traction vectors; i.e.

$$\{\bar{u}\} = \begin{Bmatrix} u_1 \\ u_2 \\ u_3 \\ V \end{Bmatrix}, \quad \{\bar{T}\} = \begin{Bmatrix} T_1 \\ T_2 \\ T_3 \\ Q \end{Bmatrix} \tag{10}$$

and the extended strains and stresses; i.e.

$$\{\bar{\varepsilon}\} = \begin{Bmatrix} \varepsilon_{11} \\ \varepsilon_{22} \\ \varepsilon_{33} \\ 2\varepsilon_{23} \\ 2\varepsilon_{31} \\ 2\varepsilon_{12} \\ -E_1 \\ -E_2 \\ -E_3 \end{Bmatrix}, \quad \{\bar{\sigma}\} = \begin{Bmatrix} \sigma_{11} \\ \sigma_{22} \\ \sigma_{33} \\ \sigma_{23} \\ \sigma_{31} \\ \sigma_{12} \\ D_1 \\ D_2 \\ D_3 \end{Bmatrix} \tag{11}$$

Eq. (9) can be reduced to the following form:

$$\int_v \rho\ddot{\bar{u}}_i\delta\bar{u}_i \, dv + \int_v \bar{\varepsilon}_s\bar{R}_{st}\delta\bar{\varepsilon}_t \, dv = \int_A \bar{T}_\alpha\delta\bar{u}_\alpha \, dA \quad \begin{cases} i = 1, \ldots, 3 \\ \alpha = 1, \ldots, 4 \\ s, t = 1, \ldots, 9 \end{cases} \tag{12}$$

where $\bar{R}$ is the extended stiffness matrix which may vary from layer to layer depending upon ply orientation and can be determined from Eqs. (3), (4), and (7). (See Appendix A).

The solutions of Eq. (12) can provide simultaneously the information on both the mechanical deformations of the structures and the electrical potentials of the distributed sensors under a given mechanical or electrical loading condition.

Finite Element Modeling

A three-dimensional finite element code, designated as "COMPZ," was developed based on Eq. (12). An eight-node, 32 degrees-of-freedom brick element that includes incompatible modes and can accommodate multi-directional layers within it was developed. It will be demonstrated that the introduction of the incompatible modes in the analysis was essential for accurately calculating the global bending response of the structure resulting from the local deformations of the piezoceramics. The multidirectional layer element can reduce considerably the amount of memory space and run time required for three-dimensional analysis of composites.

Eq. (12) can be divided into a finite number of element domains v_e within the total domain v in such a way that

$$\sum_{e=1}^{M}\left(\int_{ve} \rho\ddot{\bar{u}}_i\delta\bar{u}_i \, dv + \int_{ve} \bar{\varepsilon}_s\bar{R}_{st}\delta\bar{\varepsilon}_t \, dv\right) = \sum_{e=1}^{N}\int_{Ae} \bar{T}_\alpha\delta\bar{u}_\alpha \, dA \tag{13}$$

where M and N are the total number of elements in the domain v and along the prescribed surface A, respectively.

The extended displacements $\bar{u}_\alpha$ using the eight-node brick element shape functions together with the incompatible modes[19, 20] can be expressed as

$$\bar{u}_\alpha = \sum_{r=1}^{8} q_{\alpha r}N_r + \sum_{i=1}^{3} a_{\alpha i}P_i \tag{14}$$

where $q_{\alpha r}$ are the displacements for $\alpha = 1, 2, 3$ and voltage for $\alpha = 4$ at the nodal point r, and $a_{\alpha i}$ are the variables of the incompatible modes in the x_i direction. N_r in Eq. (14) are

the shape functions at node r[21, 22] and can be expressed in the natural coordinates (ξ, η, ζ) as

$$\begin{aligned} N_1 &= 1/8(1-\xi)(1-\eta)(1-\zeta) \\ N_2 &= 1/8(1+\xi)(1-\eta)(1-\zeta) \\ N_3 &= 1/8(1+\xi)(1+\eta)(1-\zeta) \\ N_4 &= 1/8(1-\xi)(1+\eta)(1-\zeta) \\ N_5 &= 1/8(1-\xi)(1-\eta)(1+\zeta) \\ N_6 &= 1/8(1+\xi)(1-\eta)(1+\zeta) \\ N_7 &= 1/8(1+\xi)(1+\eta)(1+\zeta) \\ N_8 &= 1/8(1-\xi)(1+\eta)(1+\zeta) \end{aligned} \tag{15}$$

where $-1 \le \xi, \eta, \zeta \le 1$, and P_i are the shape functions of the incompatible modes:

$$\begin{aligned} P_1 &= (1-\xi^2) \\ P_2 &= (1-\eta^2) \\ P_3 &= (1-\zeta^2) \end{aligned} \tag{16}$$

The relationships between the extended strains $\bar{\varepsilon}_s$ and the extended displacements $\bar{u}_\alpha$ can now be written as

$$\{\bar{\varepsilon}_s\} = \begin{Bmatrix} \varepsilon_{11} \\ \varepsilon_{22} \\ \varepsilon_{33} \\ 2\varepsilon_{23} \\ 2\varepsilon_{31} \\ 2\varepsilon_{12} \\ -E_1 \\ -E_2 \\ -E_3 \end{Bmatrix} = \begin{bmatrix} \frac{\partial}{\partial x_1} & 0 & 0 & 0 \\ 0 & \frac{\partial}{\partial x_2} & 0 & 0 \\ 0 & 0 & \frac{\partial}{\partial x_3} & 0 \\ 0 & \frac{\partial}{\partial x_3} & \frac{\partial}{\partial x_2} & 0 \\ \frac{\partial}{\partial x_3} & 0 & \frac{\partial}{\partial x_1} & 0 \\ \frac{\partial}{\partial x_2} & \frac{\partial}{\partial x_1} & 0 & 0 \\ 0 & 0 & 0 & \frac{\partial}{\partial x_1} \\ 0 & 0 & 0 & \frac{\partial}{\partial x_2} \\ 0 & 0 & 0 & \frac{\partial}{\partial x_3} \end{bmatrix} \begin{Bmatrix} u_1 \\ u_2 \\ u_3 \\ V \end{Bmatrix} \tag{17}$$

Substituting Eq. (14) into Eq. (17), we have:

$$\bar{\varepsilon}_s = \sum_{r=1}^{8} \sum_{\alpha=1}^{4} [B_{s\alpha}]_r q_{\alpha r} + \sum_{i=1}^{3} \sum_{\alpha=1}^{4} [G_{s\alpha}]_i a_{\alpha i}$$
$$s = 1, 2, \ldots, 9 \tag{18}$$

The matrices $[B_{s\alpha}]_r$ and $[G_{s\alpha}]_i$ are defined as

$$[B_{s\alpha}]_r = \begin{bmatrix} N_{r,1} & 0 & 0 & 0 \\ 0 & N_{r,2} & 0 & 0 \\ 0 & 0 & N_{r,3} & 0 \\ 0 & N_{r,3} & N_{r,2} & 0 \\ N_{r,3} & 0 & N_{r,1} & 0 \\ N_{r,2} & N_{r,1} & 0 & 0 \\ 0 & 0 & 0 & N_{r,1} \\ 0 & 0 & 0 & N_{r,2} \\ 0 & 0 & 0 & N_{r,3} \end{bmatrix}$$

$$[G_{s\alpha}]_i = \begin{bmatrix} P_{i,1} & 0 & 0 & 0 \\ 0 & P_{i,2} & 0 & 0 \\ 0 & 0 & P_{i,3} & 0 \\ 0 & P_{i,3} & P_{i,2} & 0 \\ P_{i,3} & 0 & P_{i,1} & 0 \\ P_{i,2} & P_{i,1} & 0 & 0 \\ 0 & 0 & 0 & P_{i,1} \\ 0 & 0 & 0 & P_{i,2} \\ 0 & 0 & 0 & P_{i,3} \end{bmatrix} \tag{19}$$

where r is the nodal number of the element. Each node has four degrees of freedom (u_1, u_2, u_3, and V). Accordingly, based on the standard finite element procedures,[19–22] the equilibrium equations of Eq. (13) of each element can be expressed in terms of extended nodal displacements as

$$\begin{bmatrix} M^e & 0 \\ 0 & 0 \end{bmatrix} \begin{Bmatrix} \ddot{q}^e \\ \ddot{a}^e \end{Bmatrix} + \begin{bmatrix} K^e_{qq} & K^e_{qa} \\ K^e_{aq} & K^e_{aa} \end{bmatrix} \begin{Bmatrix} q^e \\ a^e \end{Bmatrix} = \begin{Bmatrix} F^e \\ 0 \end{Bmatrix} \tag{20}$$

From the second set of Eq. (20), we have

$$\{a^e\} = -[K^e_{aa}]^{-1}[K^e_{aq}]\{q^e\} \tag{21}$$

Substituting Eq. (21) into the first set of Eq. (20) yields

$$[M^e]\{\ddot{q}^e\} + [K^e]\{q^e\} = \{F^e\} \tag{22}$$

where $[K^e]$ is defined as

$$[K^e] = [K^e_{qq}] - [K^e_{qa}][K^e_{aa}]^{-1}[K^e_{aq}] \tag{23}$$

and $[M^e]$ and $\{F^e\}$ are the mass matrix and the force vector (mechanical and electrical) of element e.

To account for the variation of the material properties through the thickness, the composite element proposed by Chang et al.[23] and Panda and Natanajan[24] was adopted. Thus, the element stiffness matrix $[K^e]$ was calculated by separately integrating each layer and summing up all the integrations:

$$[K^e_{qq}] = \sum_{k=1}^{n} \int_{-1}^{1}\int_{-1}^{1}\int_{-1}^{1} \boldsymbol{B}^T \bar{\boldsymbol{R}}^k \boldsymbol{B} |\boldsymbol{J}| \frac{h_k}{H} \, d\xi^k \, d\zeta^k \, d\eta \tag{24}$$

$$[K^e_{qa}] = \sum_{k=1}^{n} \int_{-1}^{1}\int_{-1}^{1}\int_{-1}^{1} \boldsymbol{B}^T \bar{\boldsymbol{R}}^k \boldsymbol{G} |\boldsymbol{J}| \frac{h_k}{H} \, d\xi^k \, d\zeta^k \, d\eta \tag{25}$$

$$[K^e_{aq}] = \sum_{k=1}^{n} \int_{-1}^{1}\int_{-1}^{1}\int_{-1}^{1} \boldsymbol{G}^T \bar{\boldsymbol{R}}^k \boldsymbol{B} |\boldsymbol{J}| \frac{h_k}{H} \, d\xi^k \, d\zeta^k \, d\eta \tag{26}$$

$$[K^e_{aa}] = \sum_{k=1}^{n} \int_{-1}^{1}\int_{-1}^{1}\int_{-1}^{1} \boldsymbol{G}^T \bar{\boldsymbol{R}}^k \boldsymbol{G} |\boldsymbol{J}| \frac{h_k}{H} \, d\xi^k \, d\zeta^k \, d\eta \tag{27}$$

Where $\bar{\boldsymbol{R}}^k$ is the stiffness matrix of each layer, $\boldsymbol{J}$ is the Jacobian matrix, and $\boldsymbol{B}$ and $\boldsymbol{G}$ are defined in Eq. (19). h_k is the thickness of the k-th layer within the laminate of thickness H.

To evaluate the integrals in Eqs. (24–27), Gaussian quadrature is applied to each layer. Accordingly, more than one

layer of composites with different ply orientations can be included within an element through the laminate thickness.

Each node of the element has four degrees of freedom; three normal displacements and the voltage. Substituting Eq. (22) into Eq. (13) yields

$$[M]\{\ddot{q}\} + [K]\{q\} = \{F_T\} + \{F_Q\} \tag{28}$$

where $[M]$ and $[K]$ are the mass matrix and the stiffness matrix of the entire system. $\{F_T\}$ is the mechanical force vector due to the applied traction, and $\{F_Q\}$ is the electrical force vector due to the applied charges of the actuators.

In practice, voltage may also be specified as input to the actuators. Accordingly, an additional force vector $\{F_V\}$ will be produced due to the specified voltage stored in these actuators. The corresponding electrical force vector $\{F_V\}$ can be obtained from

$$\{F_V\} = -[K_{uV}]\{q_V\} \tag{29}$$

where $[K_{uV}]$ is the stiffness matrix of these actuators containing the interaction terms between the displacements and voltage, and $\{q_V\}$ is the extended displacement vector containing specified voltages to the actuators. The derivation of Eq. (29) is given in Appendix B.

Accordingly, the finite element formulation of the equation of the equilibrium of the integrated system can be expressed as

$$[M]\{\ddot{q}\} + [K]\{q\} = \{F_T\} + \{F_Q\} + \{F_V\} \tag{30}$$

In order to consider the damping effect on the response of the structures, Rayleigh damping was assumed for the structures. Accordingly, by taking damping into account, Eq. (30) yields

$$[M]\{\ddot{q}\} + [C]\{\dot{q}\} + [k]\{q\} = \{F_T\} + \{F_Q\} + \{F_V\} \tag{31}$$

where $[C]$ is the damping matrix which can be expressed as follows:

$$[C] = a[M] + b[K] \tag{32}$$

where a and b are constants that can be determined from experiments.[21]

Accordingly, by changing the charge or voltage input to the piezoceramic actuators, the change in the configuration of the structure and the sensor voltage can be calculated from Eq. (31).

Active Control of Damping

Consider if voltage is the only electrical input to the actuators ($F_Q = 0$), Eq. (31) reduces to

$$[M]\{\ddot{q}\} + [C]\{\dot{q}\} + [K]\{q\} = \{F_T\} + \{F_V\} \tag{33}$$

For the purpose of considering the control of damping of the structure, a derivative control algorithm governing the actuating voltages $\{V\}$ may be chosen[6] as

$$\{q_V\} = [\bar{C}]\{\dot{q}\} \tag{34}$$

where $\{q\}$ may be either a displacement or a voltage vector measured at the sensor locations, and the matrix $[\bar{C}]$ is a control gain. Hence,

$$\{F_V\} = -[K_V][\bar{C}]\{\dot{q}\} = -[\tilde{C}]\{\dot{q}\} \tag{35}$$

Substituting Eq. (35) into Eq. (33) yields

$$[M]\{\ddot{q}\} + ([C] + [\tilde{C}])\{\dot{q}\} + [K]\{q\} = \{F_T\} \tag{36}$$

Now, by using a modal analysis,[22] the nodal extended displacement q is represented by

$$\{q\} = [\Phi]\{x\} \tag{37}$$

where $[\Phi]$ is the modal matrix, and $\{x\}$ are referred to as normal coordinates. The modal matrix $[\Phi]$ is simply a square matrix in which the columns correspond to the eigenvectors (the normal-mode shapes) of a system, satisfying an eigenvalue problem:

$$([K] - \omega^2[M])[\Phi] = 0 \tag{38}$$

where ω are the natural circular frequencies. Substituting Eq. (37) into Eq. (31), and then multiplying Eq. (31) with the modal matrix $[\Phi]$, we obtain the following:

$$[\Phi]^T[M][\Phi]\{\ddot{x}\} + [\Phi]^T([C] + [\tilde{C}])[\Phi]\{\dot{x}\} + [\Phi]^T[K][\Phi]\{x\} = [\Phi]^T\{F_T\} \tag{39}$$

By using the orthogonal property of the modal matrix, Eq. (39) can be written as

$$\{\ddot{x}\} + (2_{\eta\omega} + [\Phi]^T[\tilde{C}][\Phi])\{\dot{x}\} + \omega^2\{x\} = [\Phi]^T\{F_T\} \tag{40}$$

As shown in Eq. (40), the voltage control algorithm Eq. (34) has a damping effect on the structure vibration.

Therefore, the finite element analysis could be integrated with appropriately selected control algorithms to simulate the response of the structures with sensors and actuators under active control. For instance, under a given mechanical loading condition, a structure would deform accordingly, and the distributed sensor outputs could be calculated from the analysis. Then, the supply voltages to the actuators could be determined from a selected control algorithm using the calculated sensor outputs. Next, the new shape of the structure could be calculated under both the given mechanical and calculated electrical loadings. This procedure would then be iterated until the desired configuration or response of the structure has been reached.

Accordingly, two numerical examples are presented in the "Numerical Simulations" section to demonstrate how the analysis could be utilized in conjunction with control algorithms to simulate the response of integrated sensor/actuator structures. In the following section, experimental data obtained from the literature and during this investigation for verifying the computer code are presented first and compared with the numerical simulations.

Results and Comparisons

In order to verify the proposed analysis and the finite element approach, numerical calculations were generated to compare with the experimental results obtained by Crawley et. al. from a cantilevered laminated composite plate with distributed G-1195 piezoelectric ceramics bonded on the surfaces of the plate, as shown in Fig. 2.[9, 25] The dimensions of the test setup are also shown in the figure. A constant voltage with an opposite sign was applied to the piezoelectrics on each side of the plate. The deflections of the plate along the two parallel edges and the centerline were recorded by the proximity sensors, as shown in the figure.

Figure 3 shows the comparison of the deflections of a $[0/\pm 45]_S$ composite plate between the predictions and the test results. W_L, W_T and W_R in the figure are the longitudinal

bending, transverse bending, and the lateral twisting deformations, respectively, and were defined as follows:

$$W_L = \frac{M_2}{C}$$

$$W_T = \frac{M_2 - (M_1 + M_3)/2}{C}$$

$$W_R = \frac{M_1 - M_3}{C} \tag{41}$$

where C is the width of the plate, and M_1, M_2, and M_3 are the lateral deflections measured from the sensors shown in Fig. 2.

The top figure in Fig. 3 indicates the out-of-plane longitudinal bending W_L as a function of the position. The solid line is the prediction based on the model and rectangular symbols represent the experimental data. This prediction agrees with the data very well. The prediction based on the model without consideration of the incompatible modes is also presented in the figure by a dashed line. Clearly, such a prediction is completely off the scale from the data. Therefore, the inclusion of the incompatible modes in the finite element analysis is very important for analyzing this type of structure.

The transverse bending W_T and the lateral twisting W_R of the $[0/\pm 45]_S$ composite as a function of the position are shown in the middle and bottom figures of Fig. 3, respectively. In spite of the scattering of the test data, the predictions still provide reasonable accuracy as compared with the experiments. For the transverse bending mode, the model predicted that the transverse deflection converged once the position of the measurement was far enough from the clamped boundary. This prediction is consistent with intuition. For the twisting mode, the prediction was not as good as for the other modes when compared to the experiments. This can be attributed to the data being much more scattered than for the other cases and to the deformation being quite sensitive to change of material properties and geometry of the structure. Additional comparisons with Crawley's results can be found in Ha and Chang.[25]

Experiments were also performed during this investigation for further verification of the analysis and the computer simulations. T300/976 graphite/epoxy prepregs were selected for fabricating a cantilevered specimen as shown in Fig. 4. The material properties of the composites and the piezoceramics are listed in Table 1. The ply orientation of the specimen was $[0/\pm 45]_S$. Six 1.52 × 5.08 cm² PZT G1195N piezoelectric

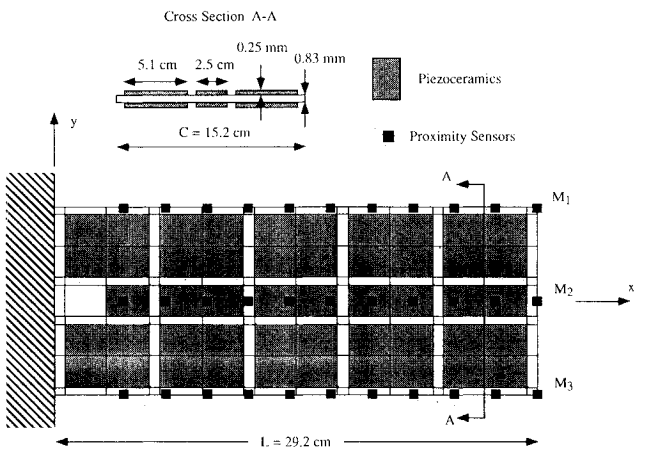

Fig. 2 Description of the experimental set-up by Crawley.[7] Cantilevered composite plate containing surface-bonded distributed piezoelectric actuators.

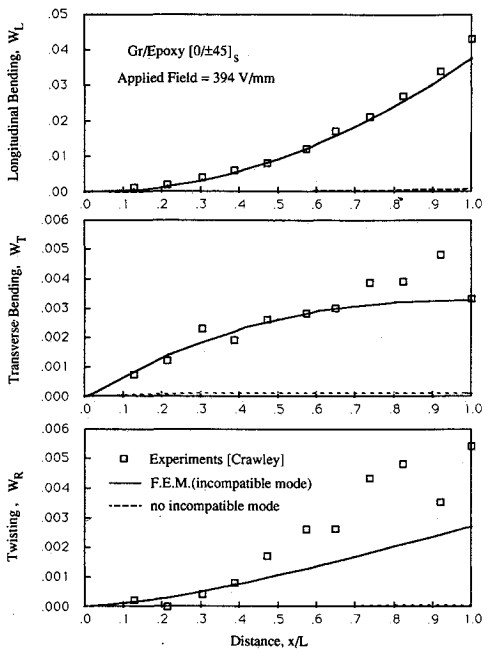

Fig. 3 Comparisons of the longitudinal bending W_L, transverse bending W_T, and lateral twisting W_R of a cantilevered $[0/\pm 45]_S$ composite plate with distributed piezoelectric actuators between the experimental measurements and the prediction based on the present analysis.

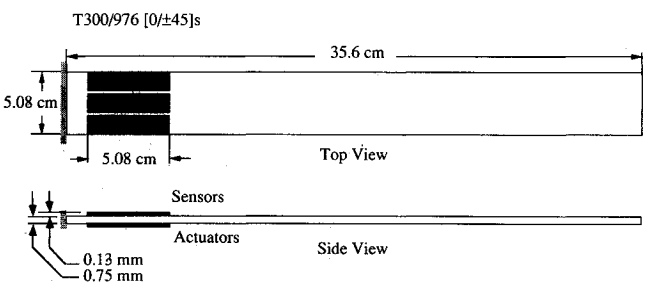

Fig. 4 Cantilever beam used in experiments with surface-bonded piezoceramics.

Table 1 Material properties of PZT G1195N piezoceramics and T300/976 graphite/epoxy unidirectional composites

	Piezoceramic	T300/976
Young's Moduli (GPa):		
E_{xx}	63.0	150.0
$E_{yy} = E_{zz}$	63.0	9.0
Poisson's ratio:		
$\nu_{xy} = \nu_{xz}$	0.3	0.3
$\nu_{zy} = \nu_{yz}$	0.3	0.3
Shear Moduli (GPa):		
$G_{xy} = G_{zx}$	24.2	7.10
G_{yz}	24.2	2.50
Density, kg/m³:		
ρ	7600	1600
Piezoelectric strain constants, pm/V:		
$d_{z1} = d_{z2}$	254	0
d_{y4}	584	0
d_{z3}	374	0
Electrical permittivity, nf/m:		
$\xi^{\sigma}_{xx} = \xi^{\sigma}_{yy}$	15.3	0
ξ^{σ}_{zz}	15.0	0
Thermal expansion coefficient, μm/m°C:		
α_x	0.9	1.1
$\alpha_y = \alpha_z$	0.9	25.2
First mode damping coefficient		
η	0	2.5×10^{-4}

ceramics were mounted near the clamped areas of the specimen. The three piezoceramics located on the upper surface of the specimen were used as sensors and the other three located on the other side as actuators.

The piezoceramics were PZT G1195N, about 0.13 mm thick. The beam was prepared for the piezoceramics by machining shallow notches to provide clearance for the back side electrical contacts, followed by light sanding and applying a zinc chromate primer. The piezoceramics were then carefully attached using a cyanacrylate adhesive. Because piezoceramics are electrically polarized, they were attached in pairs so that faces with opposite polarity were exposed on opposite sides. Each such pair was then wired in parallel after attachment.

Sensor output and actuator sine input voltages were recorded using commercially available digital data acquisition equipment (National Instruments NB-MIO-16L in a Macintosh II). The range of measurements were ± 10 V with a precision of about 5 mV. The digital sample rates were 200 Hz for step input and response, and 20 to 40 times higher than the input frequency for sine wave input and response. Sensor voltage was measured through a pair of high impedance amplifiers (about 10^{14} Ω) to minimize charge dissipation from the piezoceramics.

Figure 5 shows the typical measured sensor response of the cantilevered specimen when the actuators located at the bottom piezoceramics experienced a stepwise input of 50 V. The sensor output indicated the structure would gradually reach a steady state corresponding to an estimated averaged output voltage of -2.5 V. The averaged outputs corresponding to a steady state were recorded for the various inputs ranging from 5 to 50 V. The results of the test data are given in Fig. 6.

Numerical calculations of the sensor outputs based on the experimental condition are also presented in Fig. 6. The calculations were obtained from three different meshes, having only one, two, and six elements through the thickness. Using two and six elements through the thickness seems to produce consistent and accurate predictions and yields slightly more accurate results than the one having only one element through thickness.

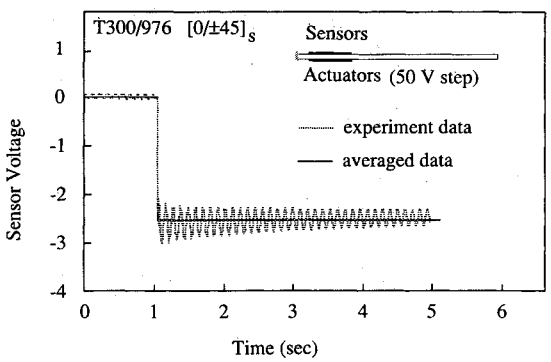

Fig. 5 Measured sensor response of a sensor/actuator composite cantilevered beam subjected to a 50 V step input on actuators.

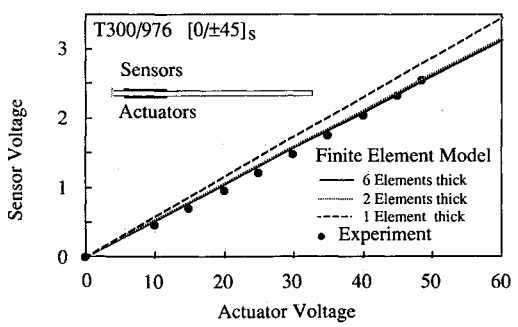

Fig. 6 Comparison of the calculated and the measured sensor response of a sensor/actuator cantilevered beam to step inputs on actuators.

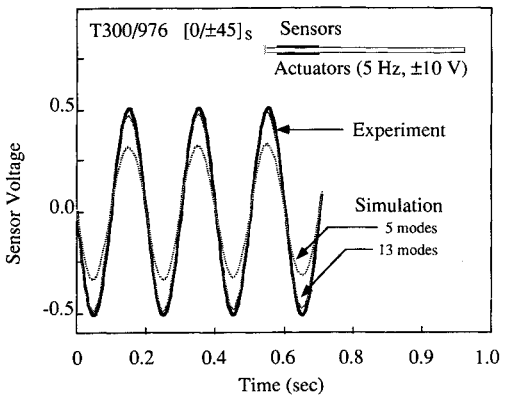

Fig. 7 Comparison of the calculated and the measured sensor response of a sensor/actuator cantilevered beam due to a 5 Hz sine input on the actuators with ± 10 V amplitude.

Table 2 National frequencies, Hz

Mode No.	Measured[a]	Calculated	Ratio[b]	Type[c,d,e]
1	9.25	9.24	1.00	B1
2	51.9	54.4	1.05	B2
3	—	76.3	—	T1
4	—	148	—	B3
5	—	243	—	T2
6	261	290	1.11	B4
7	—	438	—	BB1
8	—	446	—	T3
9	446	489	1.10	B5
10	—	697	—	T4
11	716	750	1.05	B6
12	—	1020	—	T5
13	984	1074	1.09	B7

[a]Indicates unobserved mode.
[b]Ratio is the calculated to the measured natural frequency.
[c]Type B indicates out-of-plane bending mode.
[d]Type BB indicates in-plane bending mode.
[e]Type T indicates torsion mode.

Figure 7 presents the measurements of sensor output due to the dynamic response of the cantilevered specimen, resulting from local deformations of the actuators being supplied by an input sine wave of 5 Hz frequency. The input amplitude of the voltage was 10 V. The measured output voltage from the sensors is shown in the figure. Numerical calculations of the sensor outputs were obtained from the computer code based on the modal analysis[22] using 5 and 13 modes. As a comparison, the prediction including the greater number of modes yields a better correlation than the one with fewer modes. Table 2 also lists the measured and the predicted natural frequencies of the composite beam up to thirteen modes. Due to the locations of the piezoelectric ceramics, some of the natural frequencies were not clearly measurable.

Numerical Simulations

In the following, numerical examples are presented to demonstrate the use of the computer code in conjunction with simple control algorithms for simulating the response of integrated sensor/actuator composite structures for controlling the deformations and reducing free vibration.

Shape Control

Consider a $[0/\pm 45]_S$ 22.8 × 37.2 cm^2 composite plate containing distributed piezoceramics on both upper and bottom surfaces as shown in Fig. 8. All material properties used are given in Table 1. The plate was originally flat and was simply

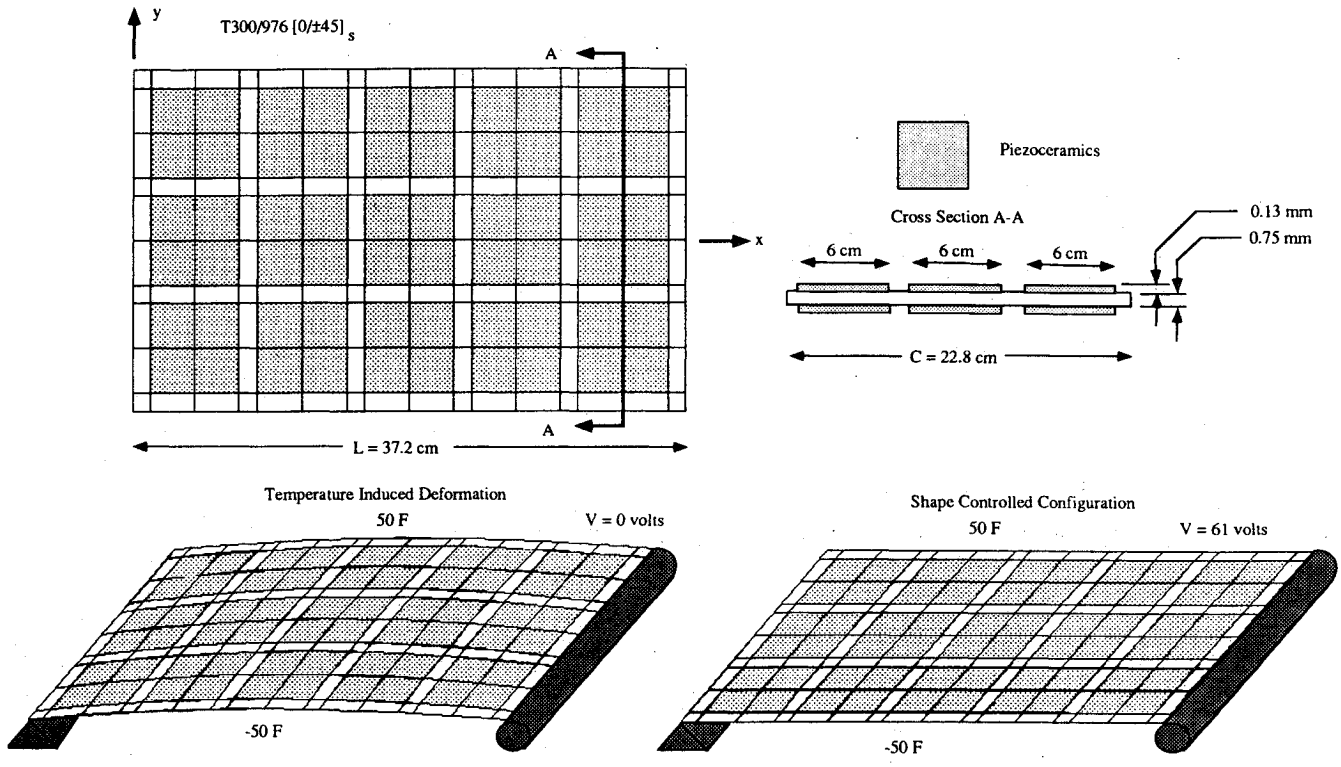

Fig. 8 Predicted configurations of an uncontrolled and a controlled actuator-composite plate exposed to elevated environment.

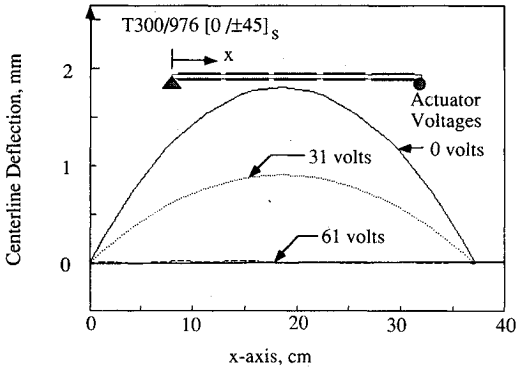

Fig. 9 Calculated centerline deflection of an actuator-composite plate exposed to elevated environment.

supported along two parallel edges and free on the other two edges.

The plate was then exposed to an elevated environment with temperature increase of 50°F on one side and with temperature drop by −50°F on the other side. It was assumed that the temperature distribution throughout the plate had reached thermal equilibrium (stationary). Due to the thermal gradient, the structure deformed into a curved shape, which can be determined from the code. The calculated deformed configuration of the structure resulting from the temperature changes was plotted along the central line of the plate and is given in Fig. 9.

The objective of the numerical simulation was to determine the amount of the electric potential to be applied to the piezoceramics such that the out-of-plane deflection of the plate could be minimized at all times. In this calculation, all of the piezoceramics were considered as actuators to control the deformations of the structure.

The calculations were performed incrementally. At each step, an amount of voltage increment required for the actuators had to be determined. It was reasonable to assume that the amount of the voltage increment ΔV required at each step would be proportional to the magnitude of the central point deflection of the plate u_o. That is:

$$\Delta V_n = \alpha \cdot u_{on} \tag{42}$$

where u_{on} is the calculated central point deflection at the n-th step and α is the active control coefficient, which has to be selected properly to assure the convergence and stability of the numerical calculations.

The total accumulated voltage V_{n+1} uniformly throughout all the actuators at the n + 1-th step is given as

$$V_{n+1} = V_n + \Delta V_n \tag{43}$$

The numerical calculations proceeded until the central deflection of the plate was reduced to a desired tolerance. Figure 9 shows the calculated centerline deflection ($x_2 = 0$) of the composite plate at the elevated environment with and without activating the piezoceramics. The solutions indicated that by supplying a constant 61 V to all the piezoceramics, the entire deformation shape of the structure was nearly flat. Other control algorithms could also be used in the code, and the number and the location of the piezoceramics to achieve the optimal design could also be evaluated by using the code.

Active Damping

The same configuration of the composite-piezoceramics plate given in Fig. 8 was considered again with only one edge rigidly fixed and all the other edges free. The ply orientation of the plate was considered to be the same as before, $[0/\pm 45]_S$. We assumed that the cantilever plate was vibrating freely under its first mode due to a past disturbance as shown in Fig. 10. The objective of the calculation was to simulate the active damping/vibration response of the plate through a simple sensor-actuator active control algorithm.

In the calculation, the central piezoceramic plate located near the clamped boundary on the bottom surface of the composite plate was chosen as the sensor. The rest of the piezoceramics were considered as actuators. To reduce actively the vibration of the plate through actuators, the amount

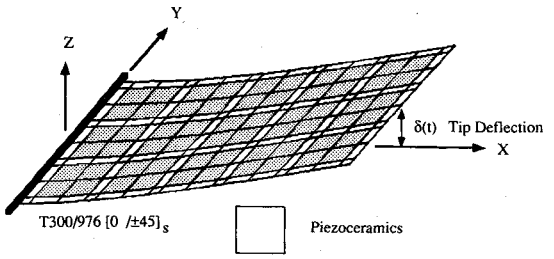

Fig. 10 Configuration of the sensor/actuator composite plate used for the first mode vibration simulation.

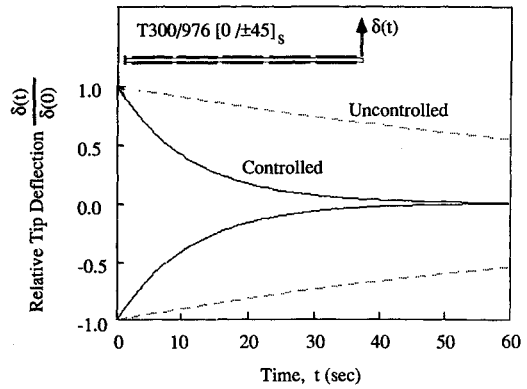

Fig. 11 Decay envelopes of tip displacement $\delta(t)$ for controlled and uncontrolled (natural) damping of a sensor/actuator composite plate subjected to first mode vibration.

of voltage supplied to the actuators had to be determined from the sensor output following a control algorithm. Here, a simple control algorithm was assumed, that the amount of input voltage to the actuators is proportional to that of the rate of sensor output and can be described as follows (see Eq. 34):

$$V_{in} = -\beta \dot{V}_{out} \tag{44}$$

where V_{in} and V_{out} are the input voltage required and output voltage measured for the actuators and sensors, respectively. β represents the control gain or the active control coefficient.

The modal analysis [Eqs. (35–40)] and the above equation were then solved to calculate the new damping factor. Here the results of the simulations of the vibration response of the cantilevered plate from the code are presented in Fig. 11, in which the dashed and solid lines show the calculated amplitudes of the central tip deflection of the plate as a function of time. The dashed lines represent the calculation with consideration for natural damping of the material only, and the solid lines resulted from the one including the additional active damping from the actuators. The results indicate that the first mode free vibration response of the plate can be efficiently controlled through the use of integrated sensor/actuator structures. It is worth noting that for modeling a coupled multiple-mode free vibration, a more sophisticated control algorithm considering inputs and outputs of multiple sensors and actuators would have to be properly selected and implemented into the code.

Conclusions

An analytical model and a computer code were developed for analyzing the mechanical-electrical response of fiber reinforced laminated composites containing distributed piezoelectric ceramics. The predictions obtained from the code correlated very well with the experiments performed during the investigation. From this study, it is believed that the computer code based on a finite element formulation could be further developed as a design tool for designing large-scale structures containing distributed sensors and actuators.

However, it is also believed that in order to simulate the response of highly integrated "smart" structures, advanced numerical techniques for efficiently integrating the structural analysis with control algorithms will be needed, and the development of appropriate control algorithms for multiple inputs and outputs of this kind would also be critically important.

Appendix A: Calculation of Extended Stiffness Matrix $\bar{R}$

Eqs. (3) and (4) can be rewritten in matrix form as

$$\{\varepsilon\} = [S]\{\sigma\} + [d]\{E\} \tag{A1}$$

$$\{D\} = [d]^T\{\sigma\} + [\xi]\{E\} \tag{A2}$$

The electric field $\{E\}$ in Eq. (A2) can be expressed as

$$\{E\} = -[\xi]^{-1}[d]^T\{\sigma\} + [\xi]^{-1}\{D\} \tag{A3}$$

Substituting Eq. (A3) into Eq. (A1) yields

$$\{\varepsilon\} = ([S] - [d][\xi]^{-1}[d]^T)\{\sigma\} + [d][\xi]^{-1}\{D\} \tag{A4}$$

From Eqs. (A3) and (A4), the extended compliance matrix $[\bar{S}]$ can be defined as

$$\{\bar{\varepsilon}\} = [\bar{S}]\{\bar{\sigma}\} \tag{A5}$$

where

$$[\bar{S}] = \begin{bmatrix} [S] - [d][\xi]^{-1}[d]^T & [d][\xi]^{-1} \\ -[\xi]^{-1}[d]^T & [\xi]^{-1} \end{bmatrix} \tag{A6}$$

The extended stiffness matrix $[\bar{R}]$ is defined as:

$$\{\bar{\sigma}\} = [\bar{R}]\{\bar{\varepsilon}\} \tag{A7}$$

From Eqs. (A5), (A6) and (A7), the extended stiffness matrix $[\bar{R}]$ can be calculated by inversing the extended compliance matrix $[\bar{S}]$:

$$[\bar{R}] = [\bar{S}]^{-1} \tag{A8}$$

For laminated composites, the extended compliance matrix $[\bar{X}]$ in Eq. (A6) simply becomes the elastic compliance $[S]$.

Appendix B: Determination of the Electrical Force Vector $\{F_V\}$

Considering the integrated sensor-actuator composite structures, the finite element formulation of the equation of equilibrium can be expressed [as given in Eq. (28)] as

$$[M]\{\ddot{q}\} + [K]\{q\} = \{F_T\} + \{F_Q\} \tag{B1}$$

More specifically, the above equation can be rearranged into the following form[15, 16]:

$$\begin{bmatrix} M_u & 0 \\ 0 & 0 \end{bmatrix}\begin{Bmatrix} \ddot{q}_u \\ \ddot{q}_V \end{Bmatrix} + \begin{bmatrix} K_u & K_{uV} \\ K_{Vu} & K_V \end{bmatrix}\begin{Bmatrix} q_u \\ q_V \end{Bmatrix} = \begin{Bmatrix} F_T \\ 0 \end{Bmatrix} + \begin{Bmatrix} 0 \\ F_Q \end{Bmatrix} \tag{B2}$$

or

$$[M_u]\{\ddot{q}_u\} + [K_u]\{q_u\} + [K_{uV}]\{q_V\} = \{F_T\} \tag{B3}$$

and

$$[K_{Vu}]\{q_u\} + [K_V]\{q_V\} = \{F_Q\} \tag{B4}$$

Here, the extended displacement $\{q\}$ is divided into two parts: $\{q_u\}$ and $\{q_V\}$, corresponding to the mechanical displacements and the voltage at the nodal points, respectively.

If $\{q_V\}$ is specified as inputs for all the actuators, the Eq. (B3) can be rewritten as

$$[M_u]\{\ddot{q}_u\} + [K_u]\{q_u\} = \{F_{Tr}\} - [K_{uV}]\{q_V\} = \{F_{Tr}\} + \{F_V\} \quad \text{(B5)}$$

when $\{F_V\} = -[K_{uV}]\{q_V\}$ is defined as the electrical force vector produced by the specified voltage vector at the actuators.

Acknowledgments

The support of the National Science Foundation through the 1988 Presidential Young Investigator Award is gratefully acknowledged. Partial support of the Charles Lee Powell Foundation grant for the program is also gratefully acknowledged.

References

[1]Tiersten, H. F., and Mindlin, R. D., "Forced Vibrations of Piezoelectric Crystal Plates," *Quarterly of Applied Mathematics*, Vol. 20, No. 10, 1962, p. 107.

[2]Zelenka, J., *Piezoelectric Resonators and Their Applications*, Elsevier, New York, 1986.

[3]Auld, B. A., *Acoustic Fields and Waves in Solids*, Vol. 1, 2nd Ed., R. E. Krieger, Melbourne, FL, 1990.

[4]Wada, B. K., "Adaptive Structures," *Proceedings of the AIAA/ASME/ASCE/AHS/ASC 30th Structures, Structural Dynamics and Materials Conference*, AIAA, New York, pp. 1–11.

[5]Wada, B. K., Fanson, J. L., and Crawley, E. F., "Adaptive Structures," *Adaptive Structures*, edited by B. K. Wada, American Society of Mechanical Engineers, 1989, pp. 1–8.

[6]Bailey, T. B., and Hubbard, J. E., Jr., "Distributed Piezoelectric-Polymer Active Vibration Control of a Cantilever Beam," *Journal of Guidance Control, and Dynamics*, Vol. 8, No. 5, 1985, pp. 605–611.

[7]Crawley, E. F., and de Luis, J., "Use of Piezoelectric Actuators as Elements of Intelligent Structures," *AIAA Journal*, Vol. 25, No. 10, 1987, pp. 1373–1385.

[8]Crawley, E. F., and Lazarus, K. B., "Induced Strain Actuation of Isotropic and Anisotropic Plates," *Proceedings of the AIAA/ASME/ASCE/AHS/ASC 30th Structures, Structural Dynamics and Materials Conference*, AIAA, New York, 1989, pp. 1451–1461.

[9]Lazarus, K. B., and Crawley, E. F., "Induced Strain Actuation Rept. of Composite Plates," GTL 197, 1989.

[10]Lee, C., Chiang, W., and O'Sullivan, T., "Piezoelectric Modal Sensors and Actuators Achieving Critical Active Damping on a Cantilevered Plate," *Proceedings of the AIAA/ASME/ASCE/AHS/ASC 30th Structures, Structural Dynamics and Materials Conference*, AIAA, New York, 1989, pp. 2018–2026.

[11]Jia, J., and Rogers, C. A., "Formulation of a Laminated Shell Theory Incorporating Embedded Distributed Actuators," *Adaptive Structures*, edited by B. K. Wada, American Society of Mechanical Engineers, 1989, pp. 25–34.

[12]Hagood, N. W., Chung, W. H., and von Flotow, A., "Modeling of Piezoelectric Actuator Dynamics for Active Structural Control," *Proceedings of the AIAA/ASME/ASCE/AHS/ASC 31st Structures, Structural Dynamics and Materials Conference*, AIAA, New York, 1990, pp. 2242–2256.

[13]Im, S., and Atluri, S. N., "Effects of a Piezo-Actuator on a Finitely Deformed Beam Subjected to General Loading," *AIAA Journal*, Vol. 27, No. 12, 1989, pp. 1801–1807.

[14]Rogers, C., Jia, J., and Liang, C., "Behavior of Shape Memory Alloy Composite Plates, Part I and II," *Proceedings of the AIAA/ASME/ASCE/AHS/ASC 30th Structures, Structural Dynamics and Materials Conference*, AIAA, New York, 1989, pp. 2011–2017, 1504–1513.

[15]Allik, H., and Hughes, T. J. R., "Finite Element Method for Piezoelectric Vibration," *International Journal for Numerical Methods in Engineering*, Vol. 2, 1970, pp. 151–157.

[16]Naillon, M., Coursant, R., and Besnier, F., "Analysis of Piezoelectric Structures by a Finite Element Method," *Acta Electronica*, Vol. 25, No. 4, 1983, pp. 341–362.

[17]Tsai, S. W., and Hahn, H. T., *Introduction to Composite Materials*, Technomic Lancaster, PA, 1980.

[18]Vinson, J. R., and Sierakowski, R. L., *The Behavior of Structures Composed of Composite Materials*, Martinus Nijhoff, Dordrecht, The Netherlands, 1987.

[19]Taylor, R. L., Beresford, P. J., and Wilson, E. L., "A Non-Conforming Element for Stress Analysis," *International Journal for Numerical Methods in Engineering*, Vol. 10, 1976, pp. 1211–1219.

[20]Wu, H. Y., and Chang, F. K., "Transient Dynamic Analysis of Laminated Composite Plates Subjected to Transverse Impact," *Computers & Structures*, Vol. 31, No. 3, 1989, pp. 453–466.

[21]Hughes, T. J. R., *The Finite Element Method*, Prentice-Hall, Englewood Cliffs, NJ, 1987.

[22]Bathe, K. J., *Finite Element Procedures in Engineering Analysis*, Prentice-Hall, Englewood Cliffs, NJ, 1982.

[23]Chang, F. K., Perez, J. L., and Chang, K. Y., "Analysis of Thick Laminated Composites," *Journal of Composite Materials*, Vol. 24, No. 8, 1990, pp. 801–822.

[24]Panda, S. C., and Natarajan, R. "Finite Element Analysis of Laminated Composite Plates," *International Journal for Numerical Methods in Engineering*, Vol. 14, No. 1, 1979, pp. 69–79.

[25]Ha, Sung K., and Chang, F. K., "Finite Element Modelling of Response of Laminated Composites with Embedded Piezoelectric Actuators," *Proceedings of the AIAA/ASME/ASCE/AHS/ASC 31st Structures, Structural Dynamics and Materials Conference*, AIAA, New York, 1990, pp. 2323–2330.